THE GLOBAL N_2O MODEL INTERCOMPARISON PROJECT

Hanqin Tian, Jia Yang, Chaoqun Lu, Rongting Xu, Josep G. Canadell, Robert B. Jackson, Almut Arneth, Jinfeng Chang, Guangsheng Chen, Philippe Ciais, Stefan Gerber, Akihiko Ito, Yuanyuan Huang, Fortunat Joos, Sebastian Lienert, Palmira Messina, Stefan Olin, Shufen Pan, Changhui Peng, Eri Saikawa, Rona L. Thompson, Nicolas Vuichard, Wilfried Winiwarter, Sönke Zaehle, Bowen Zhang, Kerou Zhang, and Qiuan Zhu

The N_2O Model Intercomparison Project (NMIP) aims at understanding and quantifying the budgets of global and regional terrestrial N_2O fluxes, environmental controls, and uncertainties associated with input data, model structure, and parameters.

Nitrous oxide (N_2O) is an important greenhouse gas (GHG), and the time-integrated radiative forcing resulting from a mass unit of N_2O is 265–298 times larger than that from carbon dioxide (CO_2) emissions for a 100-yr time horizon (Ciais et al. 2013; Myhre et al. 2013). Multiple lines of evidence indicate that human activities [e.g., industrial N_2 fixation by the Haber–Bosch process or by fossil fuel combustion and manure nitrogen (N) application] play an increasingly significant role in the perturbation of the global N cycle (Galloway et al. 2008; Gruber and Galloway 2008; Fowler et al. 2015), which has led to an increase in atmospheric N_2O concentration by ~21%, from 271 ppb at preindustrial level to 329 ppb in 2015 (MacFarling Meure et al. 2006; Prather et al. 2012, 2015; Thompson et al. 2014; www.esrl.noaa.gov/). The anthropogenic N_2O emissions are estimated to have increased from 0.7 Tg N yr^{-1} in 1860 to 6.9 Tg N yr^{-1} in 2006, ~60% of which was ascribed to agricultural activities (Ciais et al. 2013; Davidson and Kanter 2014). The increased N_2O emissions have significantly contributed to climate warming. During the 2000s, the warming effect of N_2O emissions from the terrestrial biosphere counteracted more than half of the cooling effect of the global land CO_2 sink (Tian et al. 2016), and anthropogenic N_2O emissions are projected to lead to further global warming during the twenty-first century and beyond (Stocker et al. 2013).

In terrestrial ecosystems, N_2O is mainly produced in soils via nitrification and denitrification processes (Smith and Arah 1990; Wrage et al. 2001; Schmidt et al. 2004). All these processes are regulated by microbial activities under various soil microenvironments such as soil temperature, moisture and aeration, clay content, pH, and carbon (C) and N availability (Firestone and Davidson 1989; Goldberg and Gebauer 2009; Butterbach-Bahl et al. 2013; Brotto et al. 2015; Rowlings et al. 2015). In addition, N_2O emissions from terrestrial ecosystems can be regulated by both natural disturbances and human management such as synthetic N fertilizer use, manure N application, irrigation, tillage, and the choice of crop varieties (Davidson 2009; Lu and Tian 2007; Rice and Smith 1982; Cai et al. 1997; Ding et al. 2010). However, our understanding of the mechanisms responsible for terrestrial N_2O emissions is still limited, which contributes to large uncertainties in estimating both preindustrial and contemporary N_2O emissions. For example, estimates of global terrestrial N_2O emissions from natural sources vary by up to a factor of 3 and range between 3.3 and 9.0 Tg N yr^{-1} (Ciais et al. 2013). Human-induced biogenic N_2O emissions from the land biosphere have not yet been

investigated well (Tian et al. 2016). Therefore, a major international and multidisciplinary effort is required to assess information from different research disciplines and approaches in order to constrain current knowledge on the N_2O budget and drivers and to identify research gaps.

Process-based modeling is an essential tool in assessing and predicting the terrestrial N cycle and N_2O fluxes in response to multifactor global changes. Several process-based models have been used to estimate N_2O emissions from natural and agricultural soils at various spatiotemporal scales. The conceptual model of "hole in the pipe" (Firestone and Davidson 1989) was first incorporated in the Carnegie–Ames–Stanford Approach (CASA) biosphere model (Potter et al. 1993) to estimate N trace gas emissions at the global scale (Potter et al. 1996). The daily version of the CENTURY model (DAYCENT) was linked to atmospheric models to better estimate N_2O fluxes from different ecosystems (Parton et al. 1998). The Denitrification Decomposition Model (DNDC; Li et al. 1992) was developed to study the impacts of various agricultural practices on N_2O emissions. In the Dynamic Land Ecosystem Model (DLEM), Tian et al. (2011, 2015) considered the biotic and abiotic processes (e.g., plant N uptake and N leaching loss) that regulate N_2O fluxes in natural and managed soils. In recent years, multiple C–N coupled models, such as Dynamic Nitrogen–Lund–Potsdam–Jena (DyN-LPJ; Xu-Ri and Prentice 2008), Organizing Carbon and Hydrology in Dynamic Ecosystems (ORCHIDEE) with N cycle (O-CN; Zaehle and Friend 2010, 2011), Land Surface Processes and Exchanges Model of the University of Bern (LPX-Bern 1.0; Stocker et al. 2013), Community Land Model with prognostic carbon and nitrogen (CLMCN)-N_2O (Saikawa et al. 2014), and Land Model 3V-N (LM3V-N; Huang and Gerber 2015) have been developed by integrating a prognostic N cycle into different land surface models and simulate N_2O emissions from land ecosystems. Unsurprisingly, these models generated divergent estimates of global terrestrial N_2O budgets and spatiotemporal patterns mainly owing to differences in model input datasets, model structure, and parameterization schemes. What are the major contributing factors responsible for the changing patterns of terrestrial N_2O emissions? How can we narrow down the model-estimated bias or uncertainties? What are the knowledge gaps in fully accounting for the N_2O processes? Here, we attempt to answer these questions through the establishment and designing of the global N_2O Model Intercomparison Project (NMIP).

AFFILIATIONS: Tian, Yang, Chen, and Pan—International Center for Climate and Global Change Research, School of Forestry and Wildlife Sciences, Auburn University, Auburn, Alabama, and State Key Laboratory of Urban and Regional Ecology, Research Center for Eco-Environmental Sciences, Chinese Academy of Sciences, Beijing, China; Lu—International Center for Climate and Global Change Research, School of Forestry and Wildlife Sciences, Auburn University, Auburn, Alabama, and Department of Ecology, Evolution, and Organismal Biology, Iowa State University, Ames, Iowa; Xu and B. Zhang—International Center for Climate and Global Change Research, School of Forestry and Wildlife Sciences, Auburn University, Auburn, Alabama; Canadell—Global Carbon Project, Commonwealth Scientific and Industrial Research Organisation Oceans and Atmosphere, Canberra, Australian Capital Territory, Australia; Jackson—Department of Earth System Science, Woods Institute for the Environment, and Precourt Institute for Energy, Stanford University, Stanford, California; Arneth—Karlsruhe Institute of Technology, Institute of Meteorology and Climate Research–Atmospheric Environmental Research, Garmisch-Partenkirchen, Germany; Chang, Ciais, Messina, and Vuichard—Laboratoire des Sciences du Climat et de l'Environnement, Gif sur Yvette, France; Gerber—Institute of Food and Agricultural Sciences, and Soil and Water Sciences Department, University of Florida, Gainesville, Florida; Ito—Center for Global Environmental Research, National Institute for Environmental Studies, Tsukuba, Japan; Huang—Laboratoire des Sciences du Climat et de l'Environnement, Gif sur Yvette, France, and Institute of Food and Agricultural Sciences, and Soil and Water Sciences Department, University of Florida, Gainesville, Florida; Joos and Lienert—Climate and Environmental Physics, Physics Institute, and Oeschger Centre for Climate Change Research, University of Bern, Bern, Switzerland; Olin—Department of Physical Geography and Ecosystem Science, Lund University, Lund, Sweden; Peng—Department of Biological Sciences, Université du Québec à Montréal, Montreal, Quebec, Canada, and Center for Ecological Forecasting and Global Change, College of Forestry, Northwest A&F University, Shaanxi, China; Saikawa—Department of Environmental Sciences, Emory University, Atlanta, Georgia; Thompson—Norsk Institutt for Luftforskning, Kjeller, Norway; Winiwarter—Air Quality and Greenhouse Gases, International Institute for Applied Systems Analysis, Laxenburg, Austria, and Institute of Environmental Engineering, University of Zielona Gora, Zielona Gora, Poland; Zaehle—Max Planck Institut für Biogeochemie, Jena, Germany; K. Zhang and Zhu—Center for Ecological Forecasting and Global Change, College of Forestry, Northwest A&F University, Shaanxi, China
CORRESPONDING AUTHOR: Hanqin Tian, tianhan@auburn.edu

The abstract for this article can be found in this issue, following the table of contents.

DOI:10.1175/BAMS-D-17-0212.1

In final form 27 December 2017

During the past two decades, carbon-related model intercomparison projects (MIPs) have been established to evaluate model uncertainties in simulating the terrestrial carbon dynamics. For example, the Vegetation-Ecosystem Modeling and Analysis Project (VEMAP) was a pioneer MIP activity, driven by a common model input database, and was established to provide multimodel ensemble estimates of carbon fluxes and storage in response to changing climate and atmospheric CO_2 (Melillo et al. 1995; Schimel et al. 2000). More recently, a number of CO_2-oriented MIPs and synthesis activities were implemented, such as the North American Carbon Program site and regional synthesis (NACP; Schwalm et al. 2010; Richardson et al. 2012; Schaefer et al. 2012) and its extended Multi-Scale Synthesis and Terrestrial Model Intercomparison Project (MsTMIP; Huntzinger et al. 2013; Wei et al. 2014), the Trends and Drivers of the Regional Scale Sources and Sinks of Carbon Dioxide (TRENDY) Project (Le Quéré et al. 2016; Sitch et al. 2015), the Inter-Sectoral Impact Model Intercomparison Project (ISI-MIP; Warszawski et al. 2014; Ito et al. 2016), and the Multi-Model Data Synthesis of Terrestrial Carbon Cycles in Asia (Asia-MIP; Ichii et al. 2013). These MIPs enhanced our understanding of model uncertainties and provided insight into future directions of model improvement.

Following the CO_2-related MIPs, global methane (CH_4) MIPs and synthesis activities were implemented in recent years, for example, the Wetland and Wetland CH_4 Intercomparison of Models Project (WETCHIMP; Melton et al. 2013; Wania et al. 2013) and Global Carbon Project (GCP) global CH_4 budget synthesis (Saunois et al. 2016; Poulter et al. 2017). Although terrestrial biogenic N_2O emissions significantly contribute to climate warming, the model development for simulating N cycle and N_2O fluxes remains far behind the CO_2- and CH_4-related activities. The relatively sparse and short-term observations limited our understanding of N cycling in terrestrial ecosystems. Comparing with CO_2 and CH_4, lower N_2O concentration in the atmosphere and the varying magnitudes of soil N_2O emissions across observation sites and periods make it more difficult to quantify the N_2O budget at a large scale. Another important uncertainty comes from the differences in model representation and parameterization schemes of N processes and the influence of biophysical and environmental factors on N_2O dynamics (see appendix). Similar to the purposes of the CO_2- and CH_4-related MIPs, there is a need to initialize an MIP for the N models to assess the global N_2O budget. Under the umbrella of the GCP and the International Nitrogen Initiative (INI), we initiated the NMIP to investigate the uncertainty sources in N_2O estimates and provide multimodel N_2O emissions estimates from natural and agricultural soils. This paper describes the detailed NMIP protocol, input data, model structure, and some preliminary simulation results.

THE NMIP FRAMEWORK, OBJECTIVES, AND TASKS. Motivated by large uncertainties

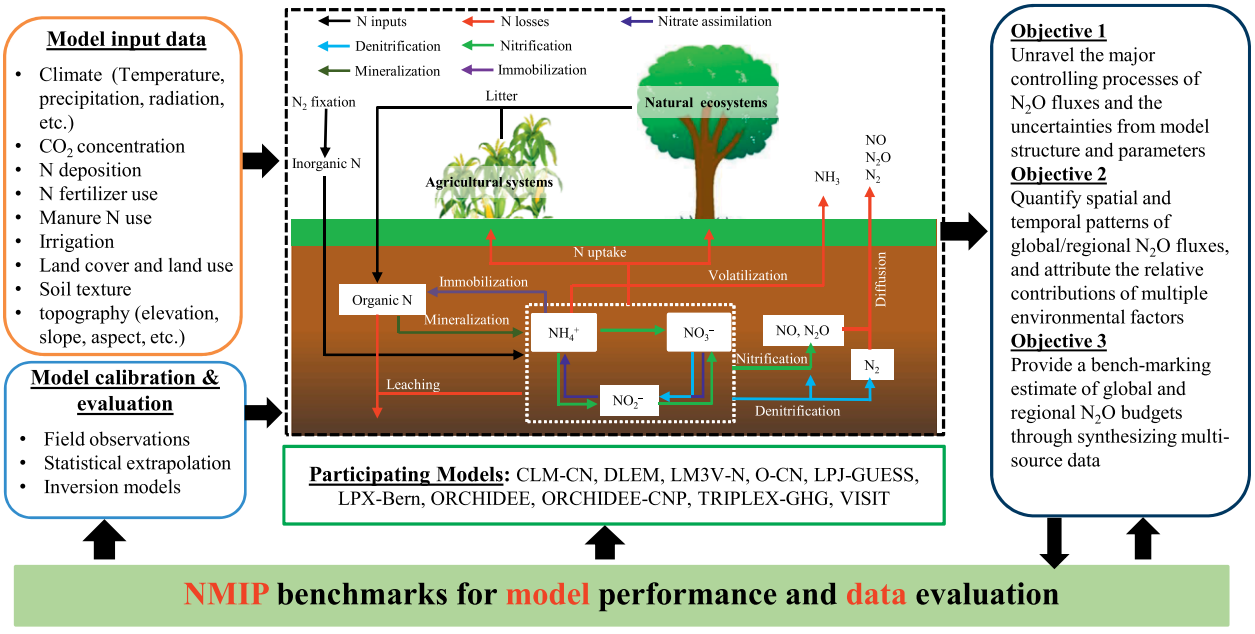

Fig. 1. The framework of NMIP.

and increasing data availability, the NMIP is developed to establish a research network for providing a multimodel ensemble estimate on the global/regional N_2O budgets and to identify major uncertainties associated with model structure, parameters, and input data (Fig. 1). This project was first proposed at the Regional Carbon Cycle Assessment and Processes (RECCAP) workshop, the Fourth International Workshop on Asian Greenhouse Gases, by JAMSTEC, in Yokohama, Japan, 8–10 April 2014. The NMIP was launched at a side meeting during the 2015 American Geophysical Union Fall Meeting and began work in the fall of 2016.

Specific objectives of NMIP are to 1) unravel the major N cycling processes controlling N_2O fluxes in each model and identify the uncertainty sources from modeling structure, input data, and parameters; 2) quantify the magnitude and spatial and temporal patterns of global and regional N_2O fluxes during 1860–2015 and attribute the relative contributions of multiple environmental factors to N_2O dynamics; and 3) provide a benchmark estimate of global/regional N_2O fluxes through synthesizing the multimodel simulation results and existing estimates from ground-based observations, inventories, and statistical/empirical extrapolations. To achieve these objectives, the NMIP group members have collectively developed a model simulation protocol as outlined in Fig. 1.

There are five key tasks or progressing stages in the protocol: 1) development and delivery of spatiotemporal model driving forces; 2) individual model calibration and evaluation; 3) model simulations and delivery of results; 4) quality control and analysis of model results; and 5) synthesis and uncertainty analysis.

KEY MODEL INPUT DATASETS. To minimize the uncertainty that results from input datasets, the NMIP provided consistent model driving datasets for all modeling groups. The datasets include potential vegetation, climate, atmospheric CO_2 concentration, atmospheric N deposition, synthetic N fertilizer applications in cropland and pasture, manure N production and applications in cropland and pasture, and historical distribution of cropland at a spatial resolution of 0.5° by 0.5° latitude–longitude (Table 1). Half-degree resolution is appropriate for studies at a global scale, considering that most of the model input data are available and many previous MIPs at a global scale were conducted at this resolution. Here we briefly describe these input datasets and their sources.

Climate. Climatic Research Unit–National Centers for Environmental Prediction (CRU–NCEP) climate version 7 is a fusion of the CRU and NCEP–NCAR reanalysis climate datasets between 1901 and 2015, which was reconstructed by the Laboratoire des Sciences du Climat et l'Environnement, Paris, France (https://vesg.ipsl.upmc.fr). Major climate variables include longwave and shortwave radiation, air pressure, humidity, temperature, precipitation, and wind speed at 6-hourly temporal resolution. Monthly magnitude of climate variables in the CRU–NCEP dataset was

Table 1. Summary of the NMIP driving forces. Note that detailed descriptions of the major NMIP model input datasets have been provided in previous publications or online documents. Here we only provide a brief description of sources and spatiotemporal patterns of these datasets.

Data name	Period	Temporal resolution	Spatial resolution	Sources	Variables
Climate	1901–2015	6-hourly	0.5°	CRU–NCEP	Incoming longwave/shortwave radiation, air humidity, pressure, precipitation, temperature, and wind speed
CO_2	1860–2015	Monthly	0.5°	NCAR	CO_2 concentration
N deposition	1860–2015	Yearly	0.5°	Eyring et al. (2013)	NH_x-N and NO_y-N deposition
N fertilizer use	1860–2014	Yearly	0.5°	Lu and Tian (2017)	N fertilizer use rate in cropland
Manure N input	1860–2014	Yearly	0.5°	B. Zhang et al. (2017)	Manure N production
Potential vegetation	One time	One time	0.5°	SYNMAP	Fraction of natural vegetation types
Cropland	1860–2015	Yearly	0.5°	HYDE 3.2	Cropland fraction

forced to be consistent with the observation-based CRU datasets.

Atmospheric CO_2. Monthly atmospheric CO_2 concentration from 1860 to 2015 was obtained from the NOAA GLOBALVIEW-CO_2 dataset derived from atmospheric and ice core measurements (www.esrl.noaa.gov).

Vegetation. Potential vegetation map was acquired from the Synergetic Land Cover Product (SYNMAP; ftp://ftp.bgc-jena.mpg.de/pub/outgoing/mjung/SYNMAP/), which merged multiple global-satellite land-cover maps into a desired classification approach (Jung et al. 2006). Each 0.5° grid cell includes the area fractions for a maximum of 47 land-cover types. Vegetation in SYNMAP is classified according to its life form, leaf type, and leaf longevity. Barren ground, permanent snow, and ice are also included in this dataset. Based on this SYNMAP dataset, participating model groups could create vegetated land fraction and reorganize the vegetation types to generate the corresponding plant functional type and fractions for their models. Annual cropland area from 1860 to 2015 was acquired from the History Database of the Global Environment, version 3.2 (HYDE 3.2), datasets (ftp://ftp.pbl.nl/hyde/), which reconstructed time-dependent land use by historical population and allocation algorithms with weighting maps (Klein Goldewijk et al. 2017). This dataset shows that global cropland area increased from 5.9 million km^2 in 1850 to 15.2 million km^2 in 2015.

Atmospheric N deposition onto land surface. The monthly atmospheric N depositions (NH_x-N and NO_y-N) during 1860–2014 were from the International Global Atmospheric Chemistry (IGAC)/Stratospheric Processes and Their Role in Climate (SPARC) Chemistry–Climate Model Initiative (CCMI) N deposition fields. CCMI models explicitly considered N emissions from natural biogenic sources, lightning, anthropogenic and biofuel sources, and biomass burning (Eyring et al. 2013). The transport of N gases was simulated by the chemical transport module in CCMI models. These data were recommended by the Coupled Model Intercomparison Project (CMIP) and used as the official products for CMIP6 models that lack interactive chemistry components (https://blogs.reading.ac.uk/ccmi/forcing-databases-in-support-of-cmip6/).

N fertilizer application. Spatially explicit synthetic N fertilizer use data were specifically developed in this project. We reconstructed the annual synthetic/mineral N fertilizer dataset from 1960 to 2014 for the global cropland, matched with HYDE 3.2 cropland distribution maps (Lu and Tian 2017; https://doi.pangaea.de/10.1594/PANGAEA.863323). Data on national-level crop-specific fertilizer use amount were collected from the International Fertilizer Industry Association (IFA) and the Food and Agriculture Organization of the United Nations (FAO). This N fertilizer dataset shows that the global total N fertilizer consumption increased from 11 Tg N yr^{-1} in 1960 to 110 Tg N yr^{-1} in 2014, and N fertilizer use rate per unit cropland area increased by about 8 times over this period. N fertilizer application rate before 1960 was linearly reduced to the zero in the 1900s.

Manure N production and application. Gridded annual manure N production in the period of 1860–2014 was developed by integrating the Global Livestock Impact Mapping System (GLIMS), the country-level livestock population from FAO, and N excretion rates of different livestock categories according to Intergovernmental Panel on Climate Change (IPCC) 2006 Tier I (B. Zhang et al. 2017; https://doi.org/10.1594/PANGAEA.871980). This annual dataset shows that manure N production increased by more than 6 times from 21 Tg N yr^{-1} in 1860 to 131 Tg N yr^{-1} in 2014, and the application rate of manure N to cropland is less than 20% of the total production. In this project, we consider the manure N application in cropland and pasture area. Manure N production and application rates in 2015 were assumed to be same as that in 2014.

All the input datasets were delivered to the modeling groups in Network Common Data Form (netCDF). To fit with individual modeling requirements for input datasets, the modeling groups could either use a subset of these datasets or add some additional datasets. For example, the participating model DLEM used all these environmental factors as inputs, while the model O-CN did not use manure N as an input. (See Table 3 for model input requirements in each model.) Figure 2 illustrates the interannual variations of the major input datasets at the global level during different available time periods. Figure 3 shows the spatial patterns of atmospheric N deposition, N fertilizer use, and manure N production in 1860, 1900, 1950, and 2015.

MODEL RESULT BENCHMARKING AND EVALUATION. Except for bottom-up model

simulations, the NMIP also plans to synthesize multiple sources of terrestrial soil N_2O emission data to provide a benchmark for evaluating model estimates. Four types of data will be collected or developed to serve as a potential benchmark: 1) site-level N cycling processes and N_2O emission measurements through chamber or eddy-flux tower across biomes; 2) N_2O flux measurement data from a national or global based measurement network [e.g., Long-Term Ecological Research Network, Long-Term Agroecosystem Research Network, Greenhouse Gas Reduction through Agriculture Carbon Enhancement Network, or the N_2O Network (www.n2o.net.au)]; 3) other spatialized datasets, including statistical extrapolation (e.g., Xu et al. 2008; Kurokawa et al. 2013; Zhuang et al. 2012); 4) N_2O fluxes from other-than-terrestrial ecosystem sources to allow for a global budget (industrial, combustion, waste water and water bodies, and marine and oceanic sources) (e.g., Battaglia and Joos 2018; Davidson and Kanter 2014; Galloway et al. 2004; Fowler et al. 2013; Winiwarter et al. 2017); and 5) atmospheric inversions (e.g., Saikawa et al. 2014; Thompson et al. 2014) in conjunction with atmospheric N_2O measurements from tall towers. We also call for more observation-derived studies to provide regional and global N_2O emission estimates through advanced computational techniques, such as machine learning, multitree ensemble (MTE), and remote sensing products. We anticipate that through multiple constraints, a process-based

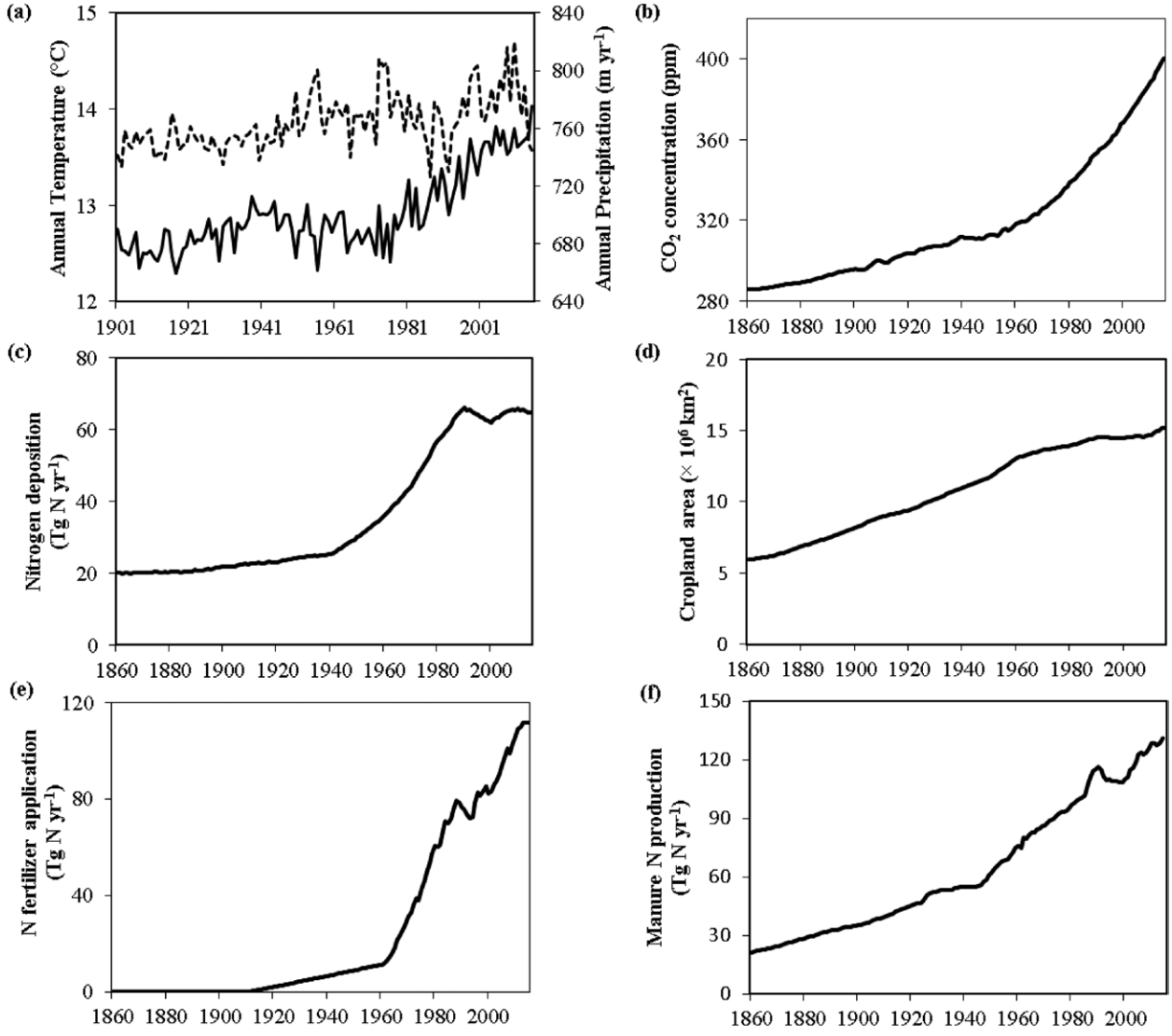

Fig. 2. Evolution of the major driving factors at the global level during 1901–2016. (a) Annual temperature (°C; solid line) and annual precipitation (mm; dashed line), (b) atmospheric CO_2 concentration (ppm), (c) N deposition (Tg N yr^{-1}), (d) cropland area (million km^2), (e) N fertilizer application (Tg N yr^{-1}), and (f) manure N production (Tg N yr^{-1}).

modeling approach can be more effective and reliable in estimating magnitude and spatial and temporal patterns of terrestrial N_2O emissions and quantifying relative contributions of environmental drivers to N_2O dynamics.

MAJOR CHARACTERISTICS OF PARTICIPATING MODELS. The N cycle in the Earth system involves complex biogeochemical processes, in which N is transformed into various chemical forms and circulates among the atmosphere, terrestrial, and aquatic ecosystems. Important terrestrial processes in the N cycle include biological N fixation (BNF), mineralization (conversion of organic N to inorganic N during the processes of organic matter decomposition), immobilization (transformation of soil inorganic N to organic N), volatilization (transformation of soil ammonium N to ammonia gas), nitrification (transformation of ammonium N to nitrate and nitrite N), denitrification (the process of nitrate/nitrite reduction by microbial activities), plant uptake from soil, resorption by living plant organs, adsorption and desorption by soil mineral particles, and N leaching from soil to aquatic systems. The modeled N processes include N transformation between organic and inorganic forms and movements among atmosphere, vegetation, soil, and riverine systems. Although N processes are tightly coupled with carbon processes in soil and vegetation, the greater variability in N processes compared to C processes makes it more difficult to simulate N cycling. At the current stage, the NMIP has included 10 ecosystem models with explicit terrestrial N cycling processes (Table 2; Fig. 1). Nine models [DLEM, LM3V-N, ORCHIDEE, ORCHIDEE with nitrogen and phosphorous cycles (ORCHIDEE-CNP), O-CN, Lund–Potsdam–Jena General Ecosystem Simulator (LPJ-GUESS), LPX-Bern, TRIPLEX-GHG, and vegetation-integrated simulator for trace gases (VISIT)] are capable of simulating N_2O emissions from both natural and agriculture ecosystems, while one model (CLM-CN) only simulates N_2O emissions from natural vegetation. The biophysical processes (such as canopy structure, albedo, and evapotranspiration), biogeochemical processes (such as decomposition and denitrification), and N input

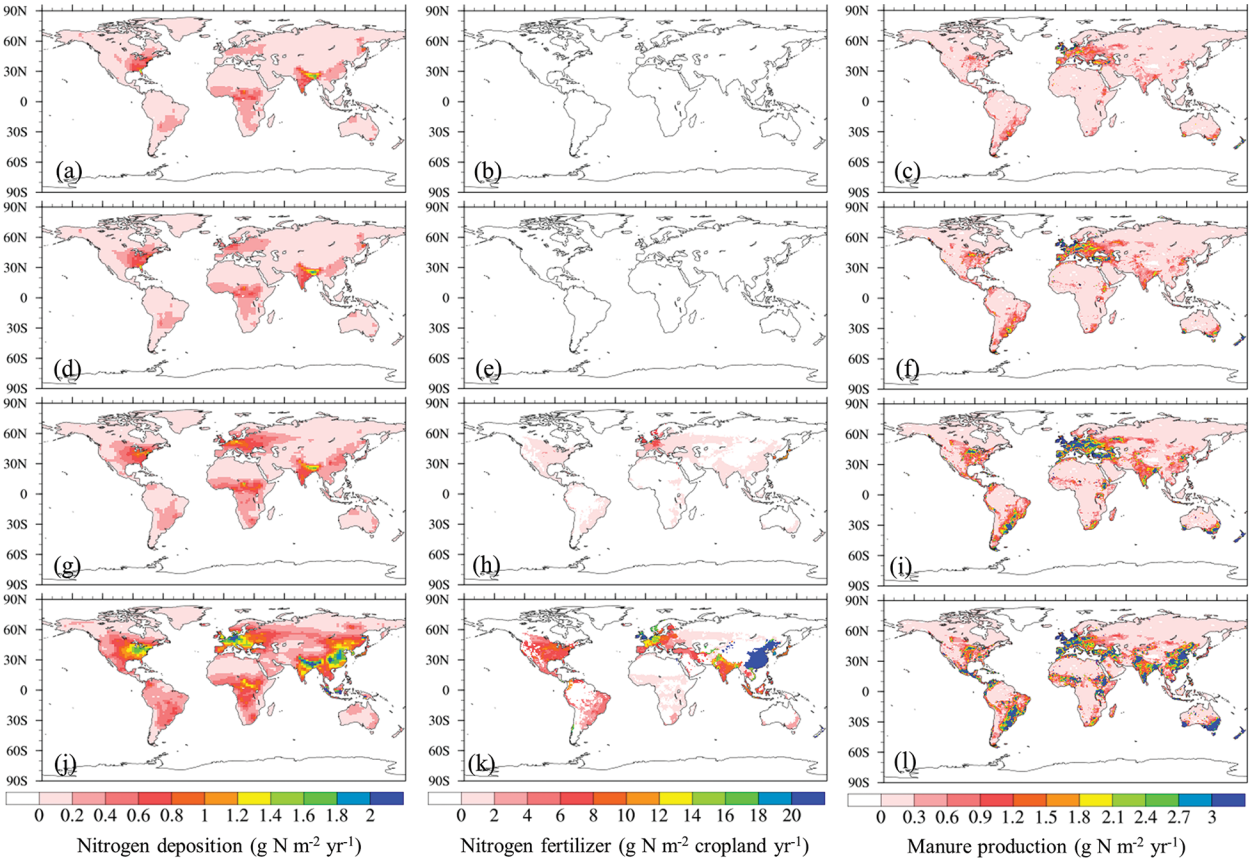

FIG. 3. Spatial distribution of (a),(d),(g),(j) N deposition (g N m^{-2} yr^{-1}); (b),(e),(h),(k) N fertilizer application (g N m^{-2} cropland yr^{-1}); and (c),(f),(i),(l) manure N production (g N m^{-2} yr^{-1}) in (first row) 1860, (second row) 1900, (third row) 1950, and (fourth row) 2015.

for cropland are significantly different from those for natural vegetation. For example, temperature in cropland was found to be lower than that in natural forest owing to the higher albedo and evapotranspiration (Bonan 2001). These differences could lead to different magnitude and timing of N_2O emissions from cropland. Therefore, biophysical characteristics and management practices in cropland, such as crop cultivation, fertilizer uses, irrigation, and harvesting, are required to be explicitly represented by the models with crop module.

To assess the uncertainty from model structure, each participating model was asked to complete a detailed survey specifying the modeling mechanisms in exogenous N inputs (e.g., N deposition, synthetic N fertilizer and manure N application, and BNF) and N transformation processes. The summarized survey results are shown in Table 3. In general, N_2O emissions from soil are regulated at two levels, which are the rates of nitrification and denitrification in the soil and soil physical factors regulating the ratio of N_2O to other nitrous gases (Davidson et al. 2000).

For N input to land ecosystems, all 10 models considered the atmospheric N deposition and biological fixation, 9 models with a crop N_2O module included N fertilizer use, but only 6 models considered manure as N input. For vegetation processes, all models included dynamic algorithms in simulating N allocation to different living tissues and vegetation N turnover and simulated plant N uptake using the "demand and supply–driven" approach. For soil N processes, all 10 models simulated N leaching according to water runoff rate; however, the models differ in representing nitrification and denitrification processes and the impacts of soil chemical and physical factors. The differences in simulating nitrification and denitrification processes are one of the major uncertainties in estimating N_2O emissions. Algorithms associated with N_2O emissions in each participating model are briefly described in the appendix.

THE NMIP MODEL SIMULATION METHODS AND EXPERIMENTAL DESIGNS. *Model initialization.* The model simulations were divided into two stages: 1) spinup and 2) transient runs (Fig. 4). During the spinup run, models were driven by the repeated climate data from 1901–20 and by other driving forces in 1860 [i.e., atmospheric CO_2 concentration, N deposition, N fertilizer use, manure N application, and land-cover and land-use change (LCLU)]. The N fertilizer use was assumed to be zero in 1860. Each model group could determine the spinup running years according to the model's specific requirement. For example, the DLEM assumed that a model reaches the equilibrium status when the differences of grid-level C, N, and water stocks were less than 0.5 g C m^{-2}, 0.5 g N m^{-2}, and 0.5 mm in two consecutive 50 years. When these thresholds were met, the spinup run stopped and the model reached an equilibrium state.

Table 2. Participating models.

Model	Contact	Affiliation	Citation
CLM-CN	E. Saikawa	Emory University	Saikawa et al. (2013)
DLEM	H. Tian	Auburn University	Tian et al. (2015); Xu et al. (2017)
LM3V-N	S. Gerber	University of Florida	Huang and Gerber (2015)
LPJ-GUESS	S. Olin/A. Arneth	Lund University, Sweden/Karlsruhe Institute of Technology, Germany	Olin et al. (2015); Xu-Ri and Prentice (2008)
LPX-Bern	S. Lienert/F. Joos	Institute for Climate and Environmental Physics, University of Bern, Switzerland	Stocker et al. (2013); Xu-Ri and Prentice (2008)
O-CN	S. Zaehle	Max Planck Institute for Biogeochemistry	Zaehle et al. (2011)
ORCHIDEE	N. Vuichard	L'Institut Pierre-Simon Laplace–Laboratoire des Sciences du Climat et de l'Environnement (IPSL–LSCE), France	N. Vuichard et al. (2018, unpublished manuscript)
ORCHIDEE-CNP	J. Chang/D. Goll	IPSL–LSCE, France	Goll et al. 2017
TRIPLEX-GHG	C. Peng	University of Quebec at Montreal, Canada	Zhu et al. (2014); K. Zhang et al. (2017)
VISIT	A. Ito	National Institute for Environmental Studies, Japan	Inatomi et al. (2010); Ito and Inatomi (2012)

Table 3. Model characteristics in simulating major N cycling processes.

	CLM-CN	DLEM	LM3V-N	LPJ -GUESS	LPX-Bern	O-CN	ORCHIDEE	ORCHIDEE-CNP	TRIPLEX-GHG	VISIT
Open N cycle[a]	Yes	Yes	Yes	Yes	Yes	Yes	Yes	Yes	Yes	Yes
C–N coupling	Yes	Yes	Yes	Yes	Yes	Yes	Yes	Yes	Yes	Yes
N pools[b]	(13, 3, 4)	(6, 6, 8)	(6, 4, 3)	(5, 6, 11)	(4,3,8)	(9, 6, 9)	(9, 6, 9)	(9, 6, 9)	(3, 9, 4)	(4, 1, 4)
Demand and supply–driven plant N uptake	Yes	Yes	Yes	Yes	Yes	Yes	Yes	Yes	Yes	Yes
N allocation[c]	Dynamic	Dynamic	Dynamic	Dynamic	Dynamic	Dynamic	Dynamic	Dynamic	Dynamic	Dynamic
Nitrification	$f(T, SWC)$	$f(T, SWC, C_{NH_4})$	$f(T, SWC, C_{NH_4})$	$f(T, SWC, C_{NH_4})$	$f(T, SWC, C_{NH_4})$	$f(T, SWC, pH, C_{NH_4})$	$f(T, SWC, pH, C_{NH_4})$	$f(T, SWC, pH, C_{NH_4})$	$f(pH, C_{NH_4}, T, SWC)$	$f(T, SWC, pH, C_{NH_4})$
Denitrification	$f(T, SWC, C_{NO_3})$	$f(T$ clay, rh, $C_{NO_3})$	$f(T_{soil}$, rh, SWC, C_{NH_4}, C_{NO_3}	$f(T$, rh, SWC, $C_{NO_3})$	$f(T, SWC, R_{mb}, C_{NO_3})$	$f(T, SWC, pH, R_{mb}, C_{NO_3})$	$f(T, SWC, pH,$ denitrifier, $C_{NO_3})$	$f(T, SWC, pH, R_{mb}, C_{NO_3})$	$f(DOC, C_{NO_3}, pH, T_{soil})$	$f(SWC,$ rh, $C_{NO_3})$
Mineralization, immobilization	f(C:N)	f(C:N)	$f(C_{NO3}, C_{NH4})$	f(C:N)	f(C:N)	f(C:N)	f(C:N)	f(C:N)	f(C:N)	f(C:N)
N leaching	f(runoff)	f(runoff)	f(runoff)	f(runoff)	f(runoff)	f(runoff, clay)	f(runoff)	f(runoff)	f(runoff)	f(runoff)
NH_3 volatilization	$f(C_{NH_4})$	f(pH, T, SWC, C_{NH_4})	f(pH, T, SWC, C_{NH_4})	f(pH, T, SWC, C_{NH_4})	f(pH, T, SWC, C_{NH_4})	$f(pH, C_{NH_4})$	$f(pH, C_{NH_4})$	$f(pH, C_{NH_4})$	$f(pH, C_{NH_4})$	f(pH, T, SWC, C_{NH_4})
Plant N turnover[d]	Dynamic	Dynamic	Dynamic	Dynamic	Dynamic	Dynamic	Dynamic	Dynamic	Dynamic	Dynamic
N resorption	f(C:N)	f(C:N)	Fixed	Crop: dynamic, the rest: fixed	$f(N_{leaf})$	Fixed	$f(N_{leaf})$	Fixed	f(C:N)	Fixed
N fixation	f(NPP)	Fixed	$f(C_{NH_4}, C_{NO_3}$, light, plant demand)	f(ET)	Implied by mass balance	$f(C_{cost}, C_{root})$	f(ET)	f(NPP)	f(biomass)	f(ET)
N fertilizer use	No	Yes	Yes	Yes	Yes	Yes	Yes	Yes	Yes	Yes
Manure N use	No	Yes	Yes	Yes	No	No	Yes	Yes	No	Yes
N deposition	Yes	Yes	Yes	Yes	Yes	Yes	Yes	Yes	Yes	Yes

[a] "Open" denotes that excess N can be leached from the system.

[b] Numbers of N pools (vegetation pools, litter pools, soil pools).

[c] Dynamic denotes time-varied N allocation ratio to different N pools.

[d] Turnover time for various vegetation nitrogen pools: soil temperature (T); soil clay fraction (denoted as clay); evapotranspiration (ET); vegetation carbon (denoted as biomass); NPP; leaf N concentration (N_{leaf}); soil surface and drainage runoff (denoted as runoff); carbon cost during N_2 fixation (C_{cost}); SWC; denitrifier: soil denitrifier biomass; soil heterogeneous respiration (rh).

Model simulation experiments. During the transient run, seven experiments were designed to simulate global terrestrial N_2O emissions. All the model experiments started with the equilibrium carbon, water, and N status in 1860, which is obtained from the spinup run, and transiently ran through the period during 1860–2015 (Fig. 4). For the period of 1860–1900 when CRU–NCEP climate data are not available, the 20-yr average climate data between 1901 and 1920 were used. In the NMIP, we applied the progressively reducing factor experimental scheme (i.e., first experiment includes all factors and then reduce one factor each time; the effect of this factor is equal to the difference between the previous and current experiment) to simulate the impacts of individual environmental factors on N_2O fluxes. In total, seven experiments (from S0 to S6) were designed (Fig. 4). The S0 reference (baseline) run was designed to track the model internal fluctuation and model drift. The S1 experiment included the temporal variations of all time-varying driving forces. "Best estimates" of N_2O emissions were acquired from either the S1 experiment (for models considering manure as input) or S2 experiment (for models without considering manure). The overall effect of all environmental factors was calculated as S1 − S0. The effects of manure N use (MANN), N fertilizer use (NFER), N deposition (NDEP), LCLU, atmospheric CO_2 (CO_2), and climate (CLIM) were calculated as S1 − S2, S2 − S3, S3 − S4, S4 − S5, S5 − S6, and S6 − S0, respectively.

MODEL OUTPUTS, QUALITY CONTROL, AND DATA AVAILABILITY. All participating model groups are requested to provide the gridded simulations of N_2O fluxes from global terrestrial ecosystems and other relevant variables that can be used for understanding C–N coupling and key N processes simulated by each individual model (Table 4). Modeling groups will submit annual simulation results during 1860-2015 and monthly simulation results during 1980-2015. In addition to modeling estimates of grid-level fluxes and pool sizes, modeling groups will submit biome-level results to facilitate biome-level N_2O emission analysis and split contributions of global N_2O dynamics to primary biome types. The model output from each modeling group is sent to the core team led by Dr. Hanqin Tian for data quality checking and preliminary analysis. The quality control is conducted to check if the individual model results are reasonable and to avoid the obvious errors during model simulations. After the quality control process, model output is transferred to a data-sharing website.

The model input and output datasets are made available to all model groups for further analyses. Model input data and model results will be made available to the broader research community once the results of the first NMIP are published. A data-use and authorship policy has been established.

RESULT ANALYSIS AND SYNTHESIS. Based on model results, the NMIP team will provide multimodel ensemble estimates for terrestrial N_2O fluxes at various scales from country, sector, continental, to global and also assess differences and uncertainties among participating models. Through the seven simulation experiments, the magnitudes and spatiotemporal variations in terrestrial N_2O emissions will be attributed to changes in different environmental factors at both regional and global scales. The global and regional N_2O flux data derived from other sources, including atmospheric inversion, statistical extrapolation, and inventory approaches [e.g., the N_2O emission data collected in Tian et al. (2016)], will be compared and integrated with the NMIP modeled results. Through these syntheses and evaluations of modeled versus field-observed N_2O dynamics, we will further identify the

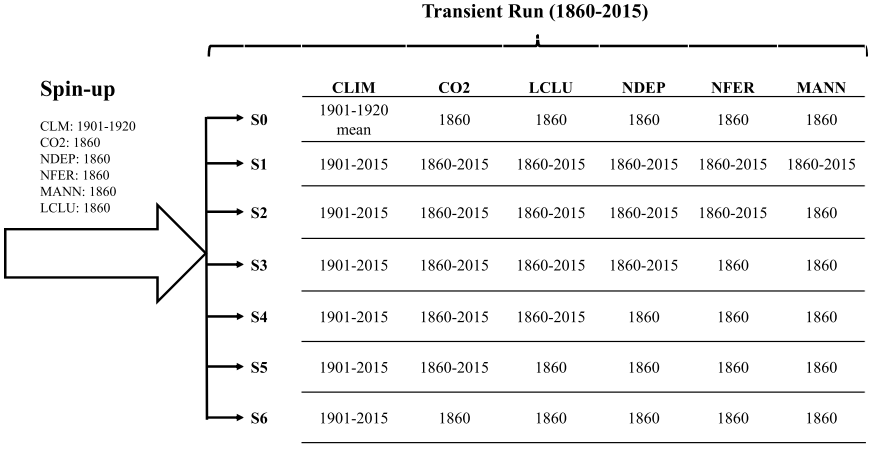

	CLIM	CO2	LCLU	NDEP	NFER	MANN
S0	1901-1920 mean	1860	1860	1860	1860	1860
S1	1901-2015	1860-2015	1860-2015	1860-2015	1860-2015	1860-2015
S2	1901-2015	1860-2015	1860-2015	1860-2015	1860-2015	1860
S3	1901-2015	1860-2015	1860-2015	1860-2015	1860	1860
S4	1901-2015	1860-2015	1860-2015	1860	1860	1860
S5	1901-2015	1860-2015	1860	1860	1860	1860
S6	1901-2015	1860	1860	1860	1860	1860

Fig. 4. Model simulation experimental designs [S0, reference (baseline); S1, climate (CLIM) + CO_2 + LCLU + NDEP + NFER + MANN; S2, CLIM + CO_2 + LCLU + NDEP + NFER; S3, CLIM + CO_2 + LCLU + NDEP; S4, CLIM + CO_2 + LCLU; S5, CLIM + CO_2; S6, CLIM). CO_2 refers to atmospheric CO_2.

Table 4. List of nitrogen and carbon variables provided by NMIP models.		
Name of variables	**Unit**	**Frequency**
Nitrogen fluxes		
N_2O flux, biological N fixation, plant N uptake (sum of ammonium and nitrate), net N mineralization, nitrification rate, denitrification rate, N leaching (Dissolved Inorganic Nitrogen, Dissolved Organic Nitrogen, Particulate Organic Nitrogen, or total N leaching), NH_3 volatilization	kg N m^{-2} s^{-1}	Monthly (1980–2015) Annual (1860–2015)
Nitrogen pools		
N in vegetation, N in above-ground litter pool, N in soil (including below-ground litter), N in products pools	kg N m^{-2}	Annual (1860–2015)
Carbon fluxes		
Gross primary production, autotrophic (plant) respiration, net primary production, heterotrophic respiration	kg C m^{-2} s^{-1}	Monthly (1980–2015) Annual (1860–2015)
Carbon pools		
C in vegetation, C in above-ground litter pool, C in soil (including below-ground litter), C in products pools, C in vegetation	kg C m^{-2}	Annual (1860–2015)

gaps in our understanding to estimate N_2O fluxes and put forward potential strategies to improve the models. In the following sections, we provide an initial analysis of simulated terrestrial N_2O emissions from the three models (DLEM, O-CN, and VISIT) that simulate both natural and agricultural emissions.

As indicated by the model ensemble, the global N_2O emission has significantly increased, especially since the 1960s with more rapidly rising exogenous N inputs to terrestrial ecosystems (Fig. 5). Natural soils were the largest source across the entire period. Cropland is the single largest contributor to the increasing trend in N_2O emissions during 1860–2015. Despite the same input datasets, the interannual variations among the three models were different because of the differences in model structure and parameters. The estimated N_2O emissions from VISIT were consistently higher than those from the other two models during 1860–2015; N_2O emissions from DLEM and O-CN were similar in magnitude. The increasing trends of N_2O emissions before the end of the 1960s were similar among the three models, while the largest increasing trend was found from O-CN, followed by DLEM, and the least from VISIT. The ultimate global terrestrial N_2O budgets, interannual variations, and attributions of the differences among models will be further analyzed in more detail after modeling results from all 10 models are included.

The terrestrial N_2O emissions showed substantial spatial variations across the global land surface since

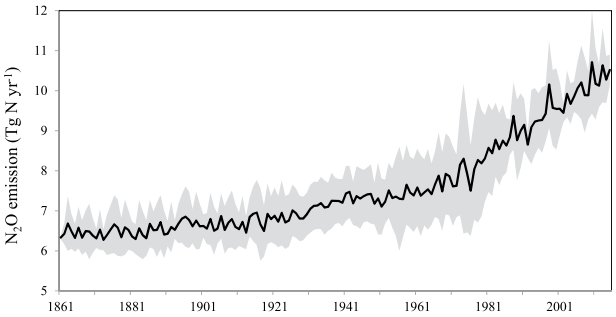

Fig. 5. Long-term trend and variations in N_2O emissions from global terrestrial ecosystems during 1861–2015 as estimated by the average of three process-based models (DLEM, O-CN, and VISIT). The gray shades denote ±1 standard deviation.

1860 (Fig. 6). The highest emission was from the tropical area during all four periods (i.e., the 1860s, 1900s, 1950s, and 2001–15) (Fig. 6), primarily owing to higher soil N transformation rates and soil N contents in tropical ecosystems. The latitudinal distribution patterns were slightly different from the 1860s to 2001–15, showing an increasing importance and the emerging second peak of N_2O emissions in the temperate climatic zone of the Northern Hemisphere. Temperate regions were another hot spot for N_2O emissions owing to the high N fertilizer use and N deposition rates in China, India, Europe, and the contiguous United States. Of all 14 examined regions as defined by GCP CH_4 budget synthesis (Saunois

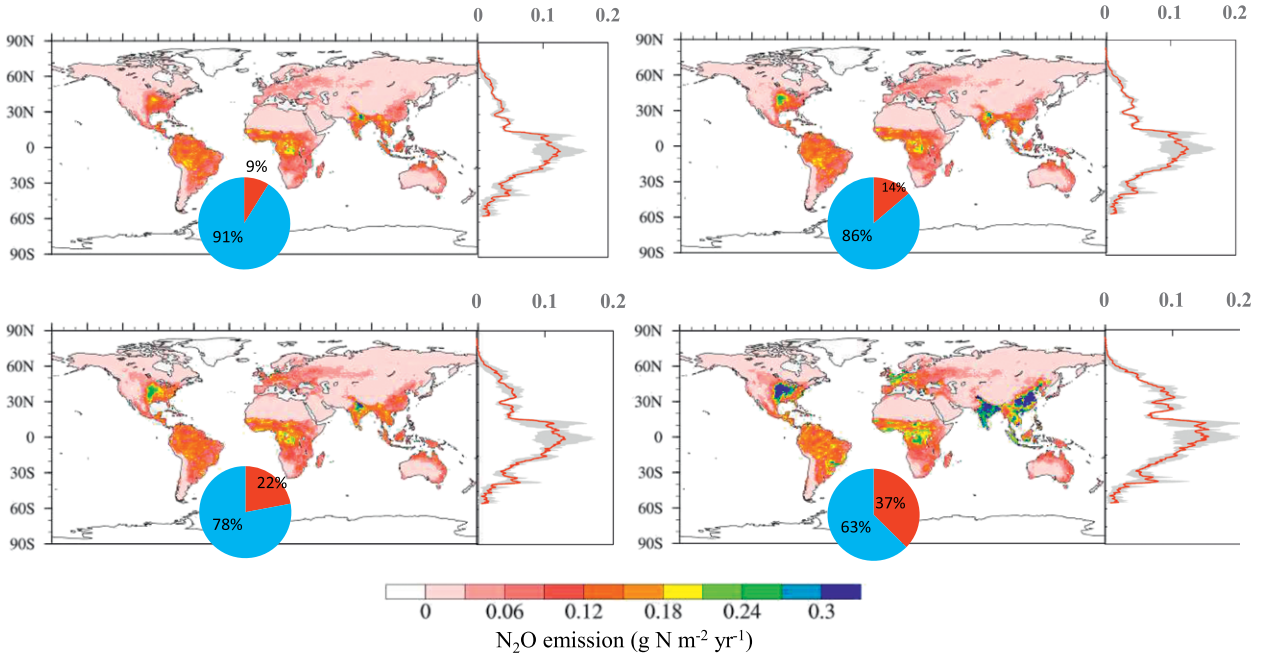

Fig. 6. Spatial patterns and the latitudinal variations of mean annual N_2O emissions as represented by the mean estimates from DLEM, VISIT, and O-CN models in the (top left) 1860s, (top right) 1900s, (bottom left) 1950s, and (bottom right) 2001–15. The pie charts indicate the relative contributions of natural vegetation (blue) and cropland (red) to the total N_2O emissions. The gray shades denote ±1 standard deviation.

et al. 2016), tropical South America had the largest N_2O emissions throughout the study period, contributing to about 20% of the global total emission (Fig. 7). China and the contiguous United States were characterized by the most rapid N_2O increasing rates increase. In the recent three decades, China, India, and western Europe were the only three regions with higher N_2O emissions from cropland than that from natural ecosystems. It is noteworthy that the estimated cropland N_2O emissions in these three regions have large uncertainty ranges due to varied model representation and parameterization methods of the impacts from agricultural management. Larger uncertainty ranges for N_2O emissions from natural ecosystems were found in Russia, northern Africa, boreal North America, Southeast Asia, and the contiguous United States.

SUMMARY. Current assessments of terrestrial N_2O emission at regional and global scales are subject to large uncertainties. The NMIP is attempting to better identify, and eventually reduce, those uncertainties. The activity was initialized in 2015 and currently includes 10 terrestrial biosphere models with N cycling coupled. NMIP is an open initiative, and other models are invited to join the effort. It aims to provide an improved estimate of global and regional terrestrial N_2O fluxes as a contribution to the larger GCP global N_2O budget synthesis activity. NMIP is being developed with the capacity to update flux estimates at regular intervals and quantify the uncertainties related to model structure, algorithms, and parameters. The NMIP protocol includes seven simulation experiments to quantify and attribute the contribution of environmental factors to the interannual variation and long-term trend of terrestrial N_2O emissions. In addition, this project intends to identify our knowledge gaps and bring forward potential strategies for improving the predictive capability of N_2O models in the future. The data products and ensemble estimates of terrestrial N_2O emissions will be made available and packaged to be relevant for policy makers and nongovernment entities participating in the climate change issues.

ACKNOWLEDGMENTS. H. Tian and his team acknowledge the support by National Key Research and Development Program of China (2017YFA0604702), CAS Grants (KFJ-STS-ZDTP-0; SKLURE2017-1-6), NOAA Grants (G00010410, G00010318), National Science Foundation (1210360, 1243232), and Auburn University IGP Program. A. Ito was supported by Japan Society for the Promotion of Science (Grant 17H01867). C. Peng acknowledges the support by National Science and Engineering Research Council of Canada (NSERC) discovery grant and China's QianRen Program. E. Saikawa

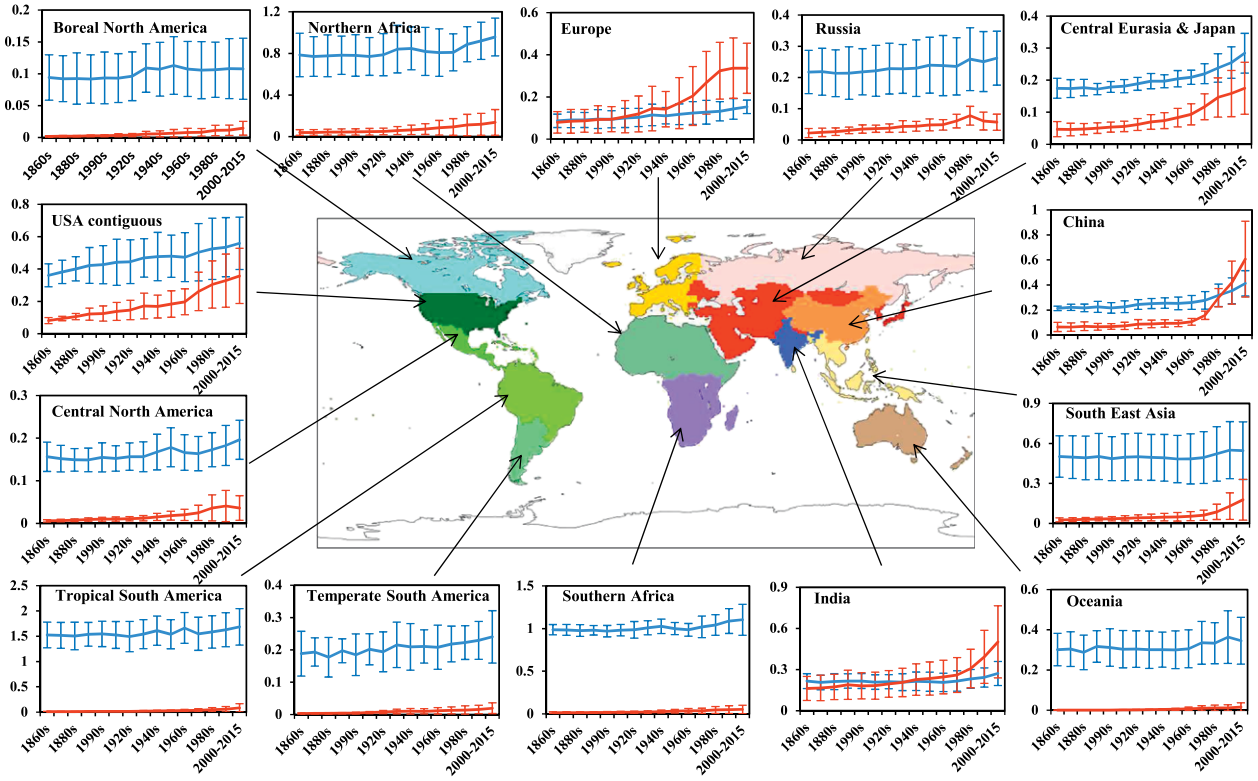

FIG. 7. Decadal N_2O emissions (Tg N yr^{-1}) from the natural ecosystems (blue lines) and cropland (red lines) in 14 regions (region delineation is from the Global Carbon Project global CH_4 budget synthesis; Saunois et al. 2016). N_2O emissions are represented by the average of DLEM, VISIT, and O-CN model simulations. The error bars denote ±1 standard deviation.

was supported by NOAA Climate Program Office's AC4 program, Award NA13OAR4310059. S. Zaehle was supported by the European Research Council (ERC) under the European Union's H2020 Programme (Grant 647304; QUINCY). P. Ciais and J. Chang are supported by the European Research Council Synergy Grant ERC-2013-SyG-610028 IMBALANCE. P. S. Lienert and F. Joos acknowledge support by the Swiss National Science Foundation (200020_172476). We acknowledge Dr. Andy Jacobson for extending global gridded monthly CO_2 data for us to use in the NMIP. The authors declare no conflict of interest.

APPENDIX: BRIEF DESCRIPTION OF ALGORITHMS ASSOCIATED WITH N_2O FLUX IN EACH PARTICIPATING MODEL.

CLM-CN-N_2O. CLM-CN-N_2O is based on the DNDC model (Li et al. 1992) implemented in the Community Land Model, version 3.5 (Oleson et al. 2008; Stöckli et al. 2008), with explicit carbon and nitrogen (CN) processes (Thornton et al. 2007; Randerson et al. 2009; Thornton et al. 2009). CLM-CN-N_2O is added to CLM-CN, version 3.5, in a one-way coupling framework and simulates N_2O emissions during nitrification and denitrification processes at an hourly time step.

Nitrification R_{nit} is temperature and moisture dependent, and N_2O is computed by the following equation as described in Li et al. (1992):

$$R_{nit} = C_{NH_4} f(T1), \quad (1)$$

where C_{NH_4} is the NH_4^+–N content in soil and $f(T1)$ is the response function of soil temperature to nitrification rate.

Denitrification is also soil temperature and moisture dependent, and it takes place under the anaerobic state. CLM-CN-N_2O specifies the anaerobic state when the water-filled pore space is more than 41.5% in the soil layer. Under this condition, N_2O is created based on the growth rate of denitrifying bacteria, as well as consumption and assimilation by plants and microbes, following Li et al. (1992). Detailed processes in simulating N_2O emissions can be found in Saikawa et al. (2013).

DLEM2.0. The nitrogen cycle schemes in DLEM2.0 (Yang et al. 2015; Xu et al. 2017; Pan et al. 2015) are similar as DLEM1.0 (Tian et al. 2010, 2011, 2012; Lu

and Tian 2013; Xu et al. 2012). However, the N_2O emission schemes in DLEM2.0 (Xu et al. 2017) have been modified based on Chatskikh et al. (2005) and Heinen (2006):

$$R_{nit} = k_{nit\_max} f(T1) f(WFPS) C_{NH_4} \text{ and} \quad (2)$$

$$R_{den} = k_{den\_max} f(T2) f(WFPS) C_{NO_3}, \quad (3)$$

where R_{nit} is the daily nitrification rate (g N m^{-2} day^{-1}); R_{den} is the daily denitrification rate (g N m^{-2} day^{-1}); f(T1) and f(T2) are the impact function of daily soil temperature on nitrification and denitrification, respectively; f(WFPS) is the impact function of water-filled pore space (WFPS) on nitrification, denitrification, and N_2O diffusion; k_{nit_max} is the maximum fraction of NH_4^+–N that is converted to NO_3^-–N or gases (0–1); k_{den_max} is the maximum fraction of NO_3^-–N that is converted to gases (0–1); and C_{NH_4} and C_{NO_3} are the soil NH_4^+–N and NO_3^-–N content (g N m^{-2}). N_2O from denitrification and nitrification processes is calculated as follows:

$$R_{N_2O} = (R_{nit} + R_{den}) f(T3)[1 - f(WFPS)], \quad (4)$$

where R_{N_2O} is the daily N_2O emission rate (g N m^{-2} day^{-1}) and f(T3) is the impact function of daily soil temperature on N_2O diffusion rate from soil pores. The calculation methods for these functions and parameters were described in detail in Xu et al. (2017) and Yang et al. (2015).

LM3V-N. In LM3V-N, nitrification is proportional to substrate availability (i.e., NH_4^+), modified by functions that account for effects of temperature and WFPS adapted from Parton et al. (1996).

Nitrification-associated N_2O emission R_{nit} is evaluated by

$$R_{nit} = k_{nit\_base} f(WFPS) f(T1) C_{NH_4} / b_{NH_4}, \quad (5)$$

where k_{nit_base} is the base nitrification rate and b_{NH_4} is the buffer parameter for soil NH_4^+.

Denitrification is described by a Monod-type equation, where both carbon and nitrate substrate availability can have limiting effects on N gas production following Li et al. (2000). These functions are further modified by temperature (based on Xu-Ri and Prentice 2008) and by WFPS indicating the availability and/or absence of oxygen (adapted from Parton et al. 1996):

$$R_{den} = k_{den\_base} f(T2) f(WFPS) f_g C_{NO3} / b_{NO3}, \quad (6)$$

where k_{den_base} is the base denitrification rate, f_g denotes the impact of labile carbon availability to nitrate on the growth of denitrifies, and b_{NO_3} is the buffer parameter for soil NO_3^-.

Gaseous losses partitioning between NO_x and N_2O during nitrification are parameterized based on air-filled porosity, following Parton et al. (2001). Partitioning between N_2O and N_2 during denitrification follows the empirical function of Del Grosso et al. (2000), which combines effects of substrate, electron donors (labile C), and water-filled pore space:

$$R_{N_2O} = 0.004 R_{nit} + R_{den} f(WFPS) f(C_{NO_3}). \quad (7)$$

Nitrification and denitrification are treated as fast processes (Shevliakova et al. 2009) and thus updated on subhourly time steps along with updates on soil moisture, soil temperature, and C and N mineralization. Model description including model formulation are detailed in Huang and Gerber (2015).

LPJ-GUESS. The nitrogen cycle scheme in LPJ-GUESS is based on CENTURY (Parton et al. 1996) and Xu-Ri and Prentice (2008). Inorganic soil nitrogen pools in the model are ammonium, nitrite, and nitrate. Nitrification occurs only in the dry part of the soil (fractionated using WFPS); the ratio between N_2O and NO_x of the gaseous losses in nitrification is based on the moisture content in the soil [f(WFPS)]:

$$R_{nit} = k_{nit\_max} f(WFPS) C_{NH_4}. \quad (8)$$

Denitrification occurs in the wet part (based on WFPS) of the soil, and the denitrification rate depends on temperature, soil moisture, and labile carbon (approximated with heterotrophic respiration rh). Gaseous losses through denitrification result in N_2O, N_2, and NO_x:

$$R_{den} = k_{den\_base} f(T2) f(WFPS) f(rh) C_{NO_3}. \quad (9)$$

The fractionation between the gaseous N species is modeled using soil moisture and temperature. All losses of gaseous N are modeled. Emissions to the atmosphere from these pools are modeled using rate modifiers that are based on the soil moisture and temperature. No retransformation of these gaseous N species is considered. These processes (N-cycling and gaseous N emissions) are modeled in different land-use classes: natural vegetation, pastures/rangelands, and croplands. On croplands, fertilizers are spread as mineral and/or organic N. Mineral fertilizers are considered as an input to the ammonium and nitrate pools at a fixed ratio (50/50) and manure as an input into the organic nitrogen pool with a fixed C:N ratio (currently set to 30).

LPX-Bern. The implementation of nitrogen dynamics in LPX-Bern is based on the work of Xu-Ri and Prentice (2008). Nitrogen uptake by plants is governed

by their demand and the availability of nitrogen in two soil pools representing ammonium and nitrate. Nitrogen from deposition and fertilization are added to these inorganic soil pools. Losses include ammonium volatilization and nitrate leaching as well as N_2O and NO production during nitrification and N_2O, NO, and N_2 production during denitrification. Aerobic nitrification of ammonium is dependent on soil temperature T_{soil} and indirectly on soil water content (SWC) owing to the partitioning of wet and dry soil:

$$R_{nit} = \max_{nit} f_1(T_{soil}) C_{NH4,dry}, \quad (10)$$

where $\max_{nit} = 0.92$ day^{-1} is the daily maximum nitrification rate at 20°C.

Anaerobic denitrification of nitrate in wet soil depends on labile carbon availability and soil temperature:

$$R_{den} = R_{mb}/(R_{mb} + K_{mb}) f_2(T_{soil}) C_{NO_3,wet} / (C_{NO_3,wet} + K_n). \quad (11)$$

The parameters K_{mb} and K_n are taken from Xu-Ri and Prentice (2008) and R_{mb} is the microbiotical soil respiration. The amount of nitrogen lost as N_2O due to nitrification and denitrification is modeled as a function of soil temperature, water content, and the respective process rate.

O-CN. The treatment of inorganic soil nitrogen dynamics in O-CN largely follows Xu-Ri and Prentice (2008). O-CN (Zaehle and Friend 2010) considers N losses to NH_3 volatilization, NO_x, N_2O, and N_2 production and emission, as well as NH_4 and NO_3 leaching. Inorganic nitrogen dynamics in the soil are tightly coupled to plant uptake and net mineralization. The anaerobic volume fraction of the soil is estimated by an empirical function of the fractional soil moisture content (Zaehle et al. 2011). The fraction of ammonium in the aerobic part of the soil is subject to nitrification, according to

$$R_{nit} = \text{vmax}_{nit} f(\text{T1}) f(\text{pH1}) C_{NH_4}, \quad (12)$$

where f(pH1) is the soil pH response functions for nitrification (Li et al. 1992; Xu-Ri and Prentice 2008) and vmax_{nit} is the maximum daily nitrification rate under 20°C and favorable pH conditions (Xu-Ri and Prentice 2008).

Gross denitrification of the fraction of nitrate under anoxic conditions is modeled as follows:

$$R_{den} = R_{mb}/(R_{mb} + K_{mb}) f(\text{T2}) f(\text{pH2}) C_{NO_3} / (C_{NO_3} + K_n), \quad (13)$$

where f(pH2) is the soil pH response functions for denitrification (Li et al. 1992; Xu-Ri and Prentice 2008), R_{mb} is the soil microbial respiration rate, and the K_{mb} and K_n parameters are taken from Li et al. (1992).

The N_2O production from nitrification and denitrification is then calculated as follows:

$$R_{N_2O} = a_{nit} f(\text{T1}) R_{nit} + b_{den} f(\text{T2}) f(\text{pH3}) R_{den}, \quad (14)$$

where a_{nit} and b_{denit} are fraction loss constants and f(pH3) is a pH modifier changing the degree of denitrification producing N_2O versus NO_x or N_2 (Zaehle et al. 2011). Emissions of volatile compounds are simulated using the empirical emission of Xu-Ri and Prentice (2008).

ORCHIDEE. Modeling of the mineral N dynamics by the ORCHIDEE model originates from the formulations used in the O-CN (Zaehle and Friend 2010). It is composed of five pools for ammonium/ammoniac, nitrate, NO_x, nitrous oxide, and dinitrogen forms. N_2O production in both nitrification and denitrification processes are represented.

The potential daily rate of nitrification R_{nit} occurs only on the aerobic fraction of the soil and is a function of temperature, pH, and ammonium concentration C_{NH_4}:

$$R_{nit} = [1 - f(\text{WFPS})] f(\text{T1}) f(\text{pH1}) k_{nit} C_{NH_4}, \quad (15)$$

where k_{nit} is the reference potential NO_3^- production per mass unit of ammonium.

N_2O production by nitrification ($R_{N_2O,nit}$, g N-N_2O m^{-2} day^{-1}) is expressed as a function of the potential daily rate of nitrification (R_{nit}, g N-NO_3^- m^{-2} day^{-1}), temperature, and the water content as shown in Zhang et al. (2002):

$$R_{N_2O,nit} = f(\text{WFPS}) f(\text{T1}) R_{nit} p_{N_2O,nit}, \quad (16)$$

where $p_{N_2O,nit}$ [g N-N_2O (g N-NO_3^-)$^{-1}$] is the reference N_2O production per mass unit of NO_3^- produced by nitrification. The denitrification occurs on the anaerobic fraction of the soil, which is computed as a function of the water-filled porosity [f(WFPS)] and is controlled by temperature, pH, soil NO concentration, and denitrifier microbial activity (a_{microb}, g m^{-2}) (Li et al. 2000):

$$R_{N_2O,den} = f(\text{WFPS}) f(\text{T2}) f(\text{pH}) f(\text{NO}) p_{N_2O,den} a_{microb}, \quad (17)$$

where f(NO) is a Michaelis–Menten shape function and $p_{N_2O,den}$ is the reference N_2O production per mass unit of denitrifier microbes.

ORCHIDEE-CNP. ORCHIDEE-CNP (Goll et al. 2017) is a version with the implementation of the phosphorus cycle into the nitrogen enabled version of

ORCHIDEE (ORCHIDEE-CN; N. Vuichard et al. 2018, unpublished manuscript). The inorganic soil nitrogen dynamics of ORCHIDEE-CNP includes N_2O from both nitrification and denitrification processes following the processes of O-CN (Zaehle et al. 2011). One exception is the BNF. In ORCHIDEE-CNP, BNF is a function of net primary production (NPP; Cleveland et al. 1999) and also regulated by soil mineral N concentration. ORCHIDEE-CNP accounts for influence of phosphorus state of vegetation on tissue nutrient concentrations and phosphatase-mediated biochemical mineralization. Changes in nutrient content (quality) of litter affect the carbon use efficiency of decomposition and in return the nutrient availability to vegetation. The model explicitly accounts for root zone depletion of phosphorus as a function of root phosphorus uptake and phosphorus transport from soil to the root surface.

TRIPLEX-GHG. The TRIPLEX-GHG model (Zhu et al. 2014; K. Zhang et al. 2017) is designed to simulate N_2O emissions by coupling major theoretical foundations for processes of nitrification and denitrification reported by Li et al. (2000). Briefly, the nitrification rate is calculated by the Michaelis–Menten function based on the concentration of NH_4^+, and microbial activity of nitrifying bacteria is explicitly involved based on simulating their growth and death; denitrification is expressed in a more complex way by taking into account the chain reaction ($NO_3^- \rightarrow NO_2^- \rightarrow NO \rightarrow N_2O \rightarrow N_2$). Each step of denitrification can be regarded as an independent process, but these steps are linked by competition for DOC between specific denitrifiers during each step. A double substrate-based (DOC and NO_x) Michaelis–Menten equation was adopted to simulate the growth rates of NO_x denitrifiers (Li et al. 2000). In addition, the effects of different factors, such as soil temperature, soil moisture, and pH, are also considered. The key equations for nitrification are as follows:

$$R_{\text{nit}} = B_{\text{nit}} \frac{R_{\max} C_{\text{NH}_4}}{(6.18 + C_{\text{NH}_4})} \text{pH}, \quad (18)$$

$$R_{\max} = \text{COE}_{\text{NR}} \times N_p, \text{ and} \quad (19)$$

$$F_{\text{N-N}_2\text{O}} = \text{FMAX}_{\text{N}_2\text{O}} R_{\text{nit}} f(\text{T1}) f(\text{WFPS}), \quad (20)$$

where R_{nit} is the nitrification rate (kg N m^{-2} day^{-1}), $R_{\max}$ is the maximum nitrification rate (day^{-1}), B_{nit} is the biomass concentration of nitrifiers (kg C m^{-2}), pH is the soil pH, COE_{NR} represents the nitrification coefficient, N_p represents the nitrification potential (mg N kg^{-1} day^{-1}), $\text{FMAX}_{\text{N}_2\text{O}}$ is the maximum N_2O fraction during nitrification (kg N m^{-2} day^{-1}), and f(T1) and f(WFPS) are the functions of the effects of soil temperature and soil moisture on N_2O emissions during nitrification, respectively.

The key equations for denitrification are showed as follows:

$$R_{\text{NO}_x} = \text{MUE}_{\text{NO}_x} \frac{[\text{DOC}]}{[\text{DOC}] + K_c} \frac{[\text{NO}_x]}{[\text{NO}_x] + K_n} \text{ and} \quad (21)$$

$$F_{\text{ANNOX}} = \text{COE}_{d\text{NO}_x} B_{\text{denit}} \left(\frac{R_{\text{NO}_x}}{\text{EFF}_{\text{NO}_x}} + \frac{\text{MAI}_{\text{NO}_x} [\text{NO}_x]}{[\text{N}]} \right) f_{\text{NO}_x}(\text{pH2}) f(\text{T2}), \quad (22)$$

where MUE_{NO_x} is the maximum growth rate of NO_x denitrifiers (h^{-1}); [DOC] and [NO_x] represent the concentrations of DOC (kg C m^{-3} h^{-1}) and NO_x (kg N m^{-3} h^{-1}), respectively, in the anaerobic balloon; and K_c (kg C m^{-3}) and K_n (kg N m^{-3}) are the half saturation value of C and N oxides, respectively. The F_{ANNOX} is the consumption rate of NO_x (kg N m^{-3} h^{-1}); $\text{COE}_{d\text{NO}_x}$ represents the coefficient of NO_x consumption; B_{denit} is the biomass of denitrifiers (kg C m^{-3}); R_{NO_x} is the NO_x reduction rate (h^{-1}); [NO_x] and [N] are the concentrations of NO_x and total N, respectively, in the anaerobic balloon (kg N m^{-3}); EFF_{NO_x} is the efficiency parameter for NO_x denitrifiers (kg C kg N^{-1}); MAI_{NO_x} is the maintenance coefficient of NO_x (h^{-1}); and $f(t)_{\text{denit}}$ represents the effect of the soil temperature on the denitrification rate during each step.

VISIT. The nitrogen cycle scheme of VISIT is composed of three organic soil nitrogen pools (microbe, litter, and humus), two inorganic soil nitrogen pools (ammonium and nitrate), and vegetation pools. Fertilizer is considered as an input to the ammonium and nitrate pools at a fixed ratio and manure as an input into the litter organic nitrogen pool. N_2O emissions through nitrification and denitrification are estimated using the scheme developed by Parton et al. (1996). Nitrification-associated N_2O emission $R_{\text{nit, N}_2\text{O}}$ is evaluated as follows:

$$R_{\text{nit, N}_2\text{O}} = f(\text{WFPS}) f(\text{pH1}) f(\text{T1}) [K_{\max} + F_{\max} f(\text{NH}_4)], \quad (23)$$

where $K_{\max}$ is the soil-specific turnover coefficient, $F_{\max}$ is the parameter of maximum nitrification gas flux, and f(NH_4) is the effect of soil ammonium on nitrification. Denitrification-associated N_2O emission $R_{\text{den, N}_2\text{O}}$ is evaluated by the following equation:

$$R_{\text{den, }N_2O} = R_{\text{den}}(1 + R_{N_2/N_2O}) \text{ and} \quad (24)$$

$$R_{\text{den}} = \min[f(NO_3^-)f(CO_2)] \times f(\text{WFPS}), \quad (25)$$

where R_{N_2/N_2O} is the fractionation coefficient, which is also a function of WFPS, soil nitrate, and heterotrophic respiration; $f(NO_3^-)$ is the maximum denitrification rate in high soil respiration rate condition; $f(CO_2)$ is the maximum denitrification rate in high NO_3^- levels; and f(WFPS) is the effect of WFPS on denitrification rate.

REFERENCES

Battaglia, G., and F. Joos, 2018: Marine N_2O emissions from nitrification and denitrification constrained by modern observations and projected in multimillennial global warming simulations. *Global Biogeochem. Cycles*, **32**, 92–121, https://doi.org/10.1002/2017GB005671.

Bonan, G. B., 2001: Observational evidence for reduction of daily maximum temperature by croplands in the Midwest United States. *J. Climate*, **14**, 2430–2442, https://doi.org/10.1175/1520-0442(2001)014<2430:OEFROD>2.0.CO;2.

Brotto, A. C., D. C. Kligerman, S. A. Andrade, R. P. Ribeiro, J. L. Oliveira, K. Chandran, and W. Z. de Mello, 2015: Factors controlling nitrous oxide emissions from a full-scale activated sludge system in the tropics. *Environ. Sci. Pollut. Res. Int.*, **22**, 11 840–11 849, https://doi.org/10.1007/s11356-015-4467-x.

Butterbach-Bahl, K., E. M. Baggs, M. Dannenmann, R. Kiese, and S. Zechmeister-Boltenstern, 2013: Nitrous oxide emissions from soils: How well do we understand the processes and their controls? *Philos. Trans. Roy. Soc. London*, **368B**, 20130122, https://doi.org/10.1098/rstb.2013.0122.

Cai, Z., G. Xing, X. Yan, H. Xu, H. Tsuruta, K. Yagi, and K. Minami, 1997: Methane and nitrous oxide emissions from rice paddy fields as affected by nitrogen fertilisers and water management. *Plant Soil*, **196**, 7–14, https://doi.org/10.1023/A:1004263405020.

Chatskikh, D., J. E. Olesen, J. Berntsen, K. Regina, and S. Yamulki, 2005: Simulation of effects of soils, climate and management on N_2O emission from grasslands. *Biogeochemistry*, **76**, 395–419, https://doi.org/10.1007/s10533-005-6996-8.

Ciais, P., and Coauthors, 2013: Carbon and other biogeochemical cycles. *Climate Change 2013: The Physical Science Basis*, T. F. Stocker et al., Eds., Cambridge University Press, 465–570.

Cleveland, C. C., and Coauthors, 1999: Global patterns of terrestrial biological nitrogen (N_2) fixation in natural ecosystems. *Global Biogeochem. Cycles*, **13**, 623–645, https://doi.org/10.1029/1999GB900014.

Davidson, E. A., 2009: The contribution of manure and fertilizer nitrogen to atmospheric nitrous oxide since 1860. *Nat. Geosci.*, **2**, 659–662, https://doi.org/10.1038/ngeo608.

——, and D. Kanter, 2014: Inventories and scenarios of nitrous oxide emissions. *Environ. Res. Lett.*, **9**, 105012, https://doi.org/10.1088/1748-9326/9/10/105012.

——, M. Keller, H. Erickson, L. Verchot, and E. Veldkamp, 2000: Testing a conceptual model of soil emissions of nitrous and nitric oxides: Using two functions based on soil nitrogen availability and soil water content, the hole-in-the-pipe model characterizes a large fraction of the observed variation of nitric oxide and nitrous oxide emissions from soils. *BioScience*, **50**, 667–680, https://doi.org/10.1641/0006-3568(2000)050[0667:TACMOS]2.0.CO;2.

Del Grosso, S., W. Parton, A. Mosier, D. Ojima, A. Kulmala, and S. Phongpan, 2000: General model for N_2O and N_2 gas emissions from soils due to dentrification. *Global Biogeochem. Cycles*, **14**, 1045–1060, https://doi.org/10.1029/1999GB001225.

Ding, W., K. Yagi, Z. Cai, and F. Han, 2010: Impact of long-term application of fertilizers on N_2O and NO production potential in an intensively cultivated sandy loam soil. *Water Air Soil Pollut.*, **212**, 141–153, https://doi.org/10.1007/s11270-010-0328-x.

Eyring, V., and Coauthors, 2013: Overview of IGAC/SPARC Chemistry-Climate Model Initiative (CCMI) community simulations in support of upcoming ozone and climate assessments. *SPARC Newsletter*, No. 40, SPARC International Project Office, Oberpfaffenhofen, Germany, 48–66, www.sparc-climate.org/fileadmin/customer/6_Publications/Newsletter_PDF/40_SPARCnewsletter_Jan2013_web.pdf.

Firestone, M. K. and E. A. Davidson, 1989: Microbiological basis of NO and N_2O production and consumption in soil. *Exchange of Trace Gases between Terrestrial Ecosystems and the Atmosphere*, M. O. Andreae and D. S. Schimel, Eds., Wiley, 7–21.

Fowler, D., and Coauthors, 2013: The global nitrogen cycle in the twenty-first century. *Philos. Trans. Roy. Soc. London*, **368B**, 20130164, https://doi.org/10.1098/rstb.2013.0164.

——, and Coauthors, 2015: Effects of global change during the 21st century on the nitrogen cycle. *Atmos. Chem. Phys.*, **15**, 13 849–13 893, https://doi.org/10.5194/acp-15-13849-2015.

Galloway, J. N., and Coauthors, 2004: Nitrogen cycles: Past, present, and future. *Biogeochemistry*, **70**, 153–226, https://doi.org/10.1007/s10533-004-0370-0.

——, and Coauthors, 2008: Transformation of the nitrogen cycle: Recent trends, questions, and potential solutions. *Science*, **320**, 889–892, https://doi.org/10.1126/science.1136674.

Goldberg, S. D., and G. Gebauer, 2009: Drought turns a central European Norway spruce forest soil from an N_2O source to a transient N_2O sink. *Global Change Biol.*, **15**, 850–860, https://doi.org/10.1111/j.1365-2486.2008.01752.x.

Goll, D. S., and Coauthors, 2017: A representation of the phosphorus cycle for ORCHIDEE. *Geosci. Model Dev.*, **10**, 3745–3770, https://doi.org/10.5194/gmd-10-3745-2017.

Gruber, N., and J. N. Galloway, 2008: An Earth-system perspective of the global nitrogen cycle. *Nature*, **451**, 293–296, https://doi.org/10.1038/nature06592.

Heinen, M., 2006: Simplified denitrification models: overview and properties. *Geoderma*, **133**, 444–463, https://doi.org/10.1016/j.geoderma.2005.06.010.

Huang, Y., and S. Gerber, 2015: Global soil nitrous oxide emissions in a dynamic carbon-nitrogen model. *Biogeosciences*, **12**, 6405–6427, https://doi.org/10.5194/bg-12-6405-2015.

Huntzinger, D. N., and Coauthors, 2013: The North American Carbon Program Multi-Scale Synthesis and Terrestrial Model Intercomparison Project: Part 1: Overview and experimental design. *Geosci. Model Dev.*, **6**, 2121–2133, https://doi.org/10.5194/gmd-6-2121-2013.

Ichii, K., and Coauthors, 2013: Site-level model–data synthesis of terrestrial carbon fluxes in the CarboEastAsia eddy-covariance observation network: Toward future modeling efforts. *J. For. Res.*, **18**, 13–20, https://doi.org/10.1007/s10310-012-0367-9.

Inatomi, M., A. Ito, K. Ishijima, and S. Murayama, 2010: Greenhouse gas budget of a cool-temperate deciduous broad-leaved forest in Japan estimated using a process-based model. *Ecosystems*, **13**, 472–483, https://doi.org/10.1007/s10021-010-9332-7.

Ito, A., and M. Inatomi, 2012: Use of a process-based model for assessing the methane budgets of global terrestrial ecosystems and evaluation of uncertainty. *Biogeosciences*, **9**, 759–773, https://doi.org/10.5194/bg-9-759-2012.

——, K. Nishina, and H. M. Noda, 2016: Evaluation of global warming impacts on the carbon budget of terrestrial ecosystems in monsoon Asia: A multi-model analysis. *Ecol. Res.*, **31**, 459–474, https://doi.org/10.1007/s11284-016-1354-y.

Jung, M., K. Henkel, M. Herold, and G. Churkina, 2006: Exploiting synergies of global land cover products for carbon cycle modeling. *Remote Sens. Environ.*, **101**, 534–553, https://doi.org/10.1016/j.rse.2006.01.020.

Klein Goldewijk, K., A. Beusen, J. Doelman, and E. Stehfest, 2017: New anthropogenic land use estimates for the Holocene; HYDE 3.2. *Earth Syst. Sci. Data*, **9**, 927–953, https://doi.org/10.5194/essd-2016-58.

Kurokawa, J., T. Ohara, T. Morikawa, S. Hanayama, G. Janssens-Maenhout, T. Fukui, K. Kawashima, and H. Akimoto, 2013: Emissions of air pollutants and greenhouse gases over Asian regions during 2000–2008: Regional Emission inventory in Asia (REAS) version 2. *Atmos. Chem. Phys.*, **13**, 11 019–11 058, https://doi.org/10.5194/acp-13-11019-2013.

Le Quéré, C., and Coauthors, 2016: Global carbon budget 2016. *Earth Syst. Sci. Data*, **8**, 605–649, https://doi.org/10.5194/essd-8-605-2016.

Li, C., S. Frolking, and T. A. Frolking, 1992: A model of nitrous oxide evolution from soil driven by rainfall events: 1. Model structure and sensitivity. *J. Geophys. Res.*, **97**, 9759–9776, https://doi.org/10.1029/92JD00509.

——, J. Aber, F. Stange, K. Butterbach-Bahl, and H. Papen, 2000: A process-oriented model of N_2O and NO emissions from forest soils: 1. Model development. *J. Geophys. Res.*, **105**, 4369–4384, https://doi.org/10.1029/1999JD900949.

Lu, C., and H. Tian, 2007: Spatial and temporal patterns of nitrogen deposition in China: Synthesis of observational data. *J. Geophys. Res.*, **112**, D22S05, https://doi.org/10.1029/2006JD007990.

——, and ——, 2013: Net greenhouse gas balance in response to nitrogen enrichment: Perspectives from a coupled biogeochemical model. *Global Change Biol.*, **19**, 571–588, https://doi.org/10.1111/gcb.12049.

——, and ——, 2017: Global nitrogen and phosphorus fertilizer use for agriculture production in the past half century: Shifted hot spots and nutrient imbalance. *Earth Syst. Sci. Data*, **9**, 181–192, https://doi.org/10.5194/essd-9-181-2017.

MacFarling Meure, M., D. Etheridge, C. Trudinger, P. Steele, R. Langenfelds, T. van Ommen, A. Smith, and J. Elkins, 2006: Law Dome CO_2, CH_4 and N_2O ice core records extended to 2000 years BP. *Geophys. Res. Lett.*, **33**, L14810, https://doi.org/10.1029/2006GL026152.

Melillo, J., J. Borchers, and J. Chaney, 1995: Vegetation/ecosystem modeling and analysis project: Comparing biogeography and geochemistry models in a continental-scale study of terrestrial ecosystem responses to climate change and CO_2 doubling. *Global Biogeochem. Cycles*, **9**, 407–437, https://doi.org/10.1029/95GB02746.

Melton, J., and Coauthors, 2013: Present state of global wetland extent and wetland methane modelling: Conclusions from a model intercomparison project

(WETCHIMP). *Biogeosciences*, **10**, 753–788, https://doi.org/10.5194/bg-10-753-2013.

Myhre, G., and Coauthors, 2013: Anthropogenic and natural radiative forcing. *Climate Change 2013: The Physical Science Basis*, T. F. Stocker et al., Eds., Cambridge University Press, 659–740.

Oleson, K., and Coauthors, 2008: Improvements to the Community Land Model and their impact on the hydrological cycle. *J. Geophys. Res.*, **113**, G01021, https://doi.org/10.1029/2007JG000563.

Olin, S., and Coauthors, 2015: Soil carbon management in large-scale Earth system modelling: Implications for crop yields and nitrogen leaching. *Earth Syst. Dyn.*, **6**, 745–768, https://doi.org/10.5194/esd-6-745-2015.

Pan, S., and Coauthors, 2015: Responses of global terrestrial evapotranspiration to climate change and increasing atmospheric CO_2 in the 21st century. *Earth's Future*, **3**, 15–35, https://doi.org/10.1002/2014EF000263.

Parton, W., A. Mosier, D. Ojima, D. Valentine, D. Schimel, K. Weier, and A. E. Kulmala, 1996: Generalized model for N_2 and N_2O production from nitrification and denitrification. *Global Biogeochem. Cycles*, **10**, 401–412, https://doi.org/10.1029/96GB01455.

——, M. Hartman, D. Ojima, and D. Schimel, 1998: DAYCENT and its land surface submodel: Description and testing. *Global Planet. Change*, **19**, 35–48, https://doi.org/10.1016/S0921-8181(98)00040-X.

——, E. Holland, S. Del Grosso, M. Hartman, R. Martin, A. Mosier, D. Ojima, and D. Schimel, 2001: Generalized model for NO_x and N_2O emissions from soils. *J. Geophys. Res.*, **106**, 17 403–17 419, https://doi.org/10.1029/2001JD900101.

Potter, C. S., J. T. Randerson, C. B. Field, P. A. Matson, P. M. Vitousek, H. A. Mooney, and S. A. Klooster, 1993: Terrestrial ecosystem production: A process model based on global satellite and surface data. *Global Biogeochem. Cycles*, **7**, 811–841, https://doi.org/10.1029/93GB02725.

——, P. A. Matson, P. M. Vitousek, and E. A. Davidson, 1996: Process modeling of controls on nitrogen trace gas emissions from soils worldwide. *J. Geophys. Res.*, **101**, 1361–1377, https://doi.org/10.1029/95JD02028.

Poulter, B., and Coauthors, 2017: Global wetland contribution to 2000–2012 atmospheric methane growth rate dynamics. *Environ. Res. Lett.*, **12**, 094013, https://doi.org/10.1088/1748-9326/aa8391.

Prather, M. J., C. D. Holmes, and J. Hsu, 2012: Reactive greenhouse gas scenarios: Systematic exploration of uncertainties and the role of atmospheric chemistry. *Geophys. Res. Lett.*, **39**, L09803, https://doi.org/10.1029/2012GL051440.

——, and Coauthors, 2015: Measuring and modeling the lifetime of nitrous oxide including its variability. *J. Geophys. Res. Atmos.*, **120**, 5693–5705, https://doi.org/10.1002/2015JD023267.

Randerson, J. T., and Coauthors, 2009: Systematic assessment of terrestrial biogeochemistry in coupled climate–carbon models. *Global Change Biol.*, **15**, 2462–2484, https://doi.org/10.1111/j.1365-2486.2009.01912.x.

Rice, C. W., and M. S. Smith, 1982: Denitrification in no-till and plowed soils. *Soil Sci. Soc. Amer. J.*, **46**, 1168–1173, https://doi.org/10.2136/sssaj1982.03615995004600060010x.

Richardson, A. D., and Coauthors, 2012: Terrestrial biosphere models need better representation of vegetation phenology: Results from the North American carbon program site synthesis. *Global Change Biol.*, **18**, 566–584, https://doi.org/10.1111/j.1365-2486.2011.02562.x.

Rowlings, D., P. Grace, C. Scheer, and S. Liu, 2015: Rainfall variability drives interannual variation in N_2O emissions from a humid, subtropical pasture. *Sci. Total Environ.*, **512**, 8–18, https://doi.org/10.1016/j.scitotenv.2015.01.011.

Saikawa, E., C. Schlosser, and R. Prinn, 2013: Global modeling of soil nitrous oxide emissions from natural processes. *Global Biogeochem. Cycles*, **27**, 972–989, https://doi.org/10.1002/gbc.20087.

——, and Coauthors, 2014: Global and regional emissions estimates for N_2O. *Atmos. Chem. Phys.*, **14**, 4617–4641, https://doi.org/10.5194/acp-14-4617-2014.

Saunois, M., and Coauthors, 2016: The global methane budget 2000–2012. *Earth Syst. Sci. Data*, **8**, 697–751, https://doi.org/10.5194/essd-8-697-2016.

Schaefer, K., and Coauthors, 2012: A model-data comparison of gross primary productivity: Results from the North American Carbon Program site synthesis. *J. Geophys. Res.*, **117**, G03010, https://doi.org/10.1029/2012JG001960.

Schimel, D., and Coauthors, 2000: Contribution of increasing CO_2 and climate to carbon storage by ecosystems in the United States. *Science*, **287**, 2004–2006, https://doi.org/10.1126/science.287.5460.2004.

Schmidt, I., R. J. van Spanning, and M. S. Jetten, 2004: Denitrification and ammonia oxidation by *Nitrosomonas europaea* wild-type, and NirK-and NorB-deficient mutants. *Microbiology*, **150**, 4107–4114, https://doi.org/10.1099/mic.0.27382-0.

Schwalm, C. R., and Coauthors, 2010: A model-data intercomparison of CO_2 exchange across North America: Results from the North American Carbon Program site synthesis. *J. Geophys. Res.*, **115**, G00H05, https://doi.org/10.1029/2009JG001229.

Shevliakova, E., and Coauthors, 2009: Carbon cycling under 300 years of land use change: Importance of the secondary vegetation sink. *Global Biogeochem. Cycles*, **23**, GB2022, https://doi.org/10.1029/2007GB003176.

Sitch, S., and Coauthors, 2015: Recent trends and drivers of regional sources and sinks of carbon dioxide. *Biogeosciences*, **12**, 653–679, https://doi.org/10.5194/bg-12-653-2015.

Smith, K. A., and J. Arah, 1990: Losses of nitrogen by denitrification and emissions of nitrogen oxides from soils. *Proc. Fert. Soc.*, **299**, 34 pp.

Stocker, B. D., R. Roth, F. Joos, R. Spahni, M. Steinacher, S. Zaehle, L. Bouwman, and I. C. Prentice, 2013: Multiple greenhouse-gas feedbacks from the land biosphere under future climate change scenarios. *Nat. Climate Change*, **3**, 666–672, https://doi.org/10.1038/nclimate1864.

Stöckli, R., and Coauthors, 2008: Use of FLUXNET in the Community Land Model development. *J. Geophys. Res.*, **113**, G01025, https://doi.org/10.1029/2007JG000562.

Thompson, R. L., and Coauthors, 2014: TransCom N_2O model inter-comparison—Part 2: Atmospheric inversion estimates of N_2O emissions. *Atmos. Chem. Phys.*, **14**, 6177–6194, https://doi.org/10.5194/acp-14-6177-2014.

Thornton, P. E., J. F. Lamarque, N. A. Rosenbloom, and N. M. Mahowald, 2007: Influence of carbon-nitrogen cycle coupling on land model response to CO_2 fertilization and climate variability. *Global Biogeochem. Cycles*, **21**, GB4018, https://doi.org/10.1029/2006GB002868.

——, and Coauthors, 2009: Carbon-nitrogen interactions regulate climate-carbon cycle feedbacks: results from an atmosphere-ocean general circulation model. *Biogeosciences*, **6**, 2099–2120, https://doi.org/10.5194/bg-6-2099-2009.

Tian, H., X. Xu, M. Liu, W. Ren, C. Zhang, G. Chen, and C. Lu, 2010: Spatial and temporal patterns of CH_4 and N_2O fluxes in terrestrial ecosystems of North America during 1979–2008: Application of a global biogeochemistry model. *Biogeosciences*, **7**, 2673–2694, https://doi.org/10.5194/bg-7-2673-2010.

——, ——, C. Lu, M. Liu, W. Ren, G. Chen, J. Melillo, and J. Liu, 2011: Net exchanges of CO_2, CH_4, and N_2O between China's terrestrial ecosystems and the atmosphere and their contributions to global climate warming. *J. Geophys. Res.*, **116**, G02011, https://doi.org/10.1029/2010JG001393.

——, and Coauthors, 2012: Century-scale responses of ecosystem carbon storage and flux to multiple environmental changes in the southern United States. *Ecosystems*, **15**, 674–694, https://doi.org/10.1007/s10021-012-9539-x.

——, and Coauthors, 2015: Global methane and nitrous oxide emissions from terrestrial ecosystems due to multiple environmental changes. *Ecosyst. Health Sustain.*, **1**, 1–20, https://doi.org/10.1890/EHS14-0015.1.

——, and Coauthors, 2016: The terrestrial biosphere as a net source of greenhouse gases to the atmosphere. *Nature*, **531**, 225–228, https://doi.org/10.1038/nature16946.

Wania, R., and Coauthors, 2013: Present state of global wetland extent and wetland methane modelling: Methodology of a model inter-comparison project (WETCHIMP). *Geosci. Model Dev.*, **6**, 617–641, https://doi.org/10.5194/gmd-6-617-2013.

Warszawski, L., K. Frieler, V. Huber, F. Piontek, O. Serdeczny, and J. Schewe, 2014: The inter-sectoral impact model intercomparison project (ISI–MIP): Project framework. *Proc. Natl. Acad. Sci. USA*, **111**, 3228–3232, https://doi.org/10.1073/pnas.1312330110.

Wei, Y., and Coauthors, 2014: The North American Carbon Program Multi-Scale Synthesis and Terrestrial Model Intercomparison Project—Part 2: Environmental driver data. *Geosci. Model Dev.*, **7**, 2875–2893, https://doi.org/10.5194/gmd-7-2875-2014.

Winiwarter, W., L. Höglund-Isaksson, Z. Klimont, W. Schöpp, and M. Amann, 2017: Technical opportunities to reduce global anthropogenic emissions of nitrous oxide. *Environ. Res. Lett.*, **13**, 014011, https://doi.org/10.1088/1748-9326/aa9ec9.

Wrage, N., G. Velthof, M. Van Beusichem, and O. Oenema, 2001: Role of nitrifier denitrification in the production of nitrous oxide. *Soil Biol. Biochem.*, **33**, 1723–1732, https://doi.org/10.1016/S0038-0717(01)00096-7.

Xu, R., H. Tian, C. Lu, S. Pan, J. Chen, J. Yang, and B. Zhang, 2017: Preindustrial nitrous oxide emissions from the land biosphere estimated by using a global biogeochemistry model. *Climate Past*, **13**, 977–990, https://doi.org/10.5194/cp-13-977-2017.

Xu, X., H. Tian, G. Chen, M. Liu, W. Ren, C. Lu, and C. Zhang, 2012: Multifactor controls on terrestrial N_2O flux over North America from 1979 through 2010. *Biogeosciences*, **9**, 1351–1366, https://doi.org/10.5194/bg-9-1351-2012.

Xu-Ri, and I. C. Prentice, 2008: Terrestrial nitrogen cycle simulation with a dynamic global vegetation model. *Global Change Biol.*, **14**, 1745–1764, https://doi.org/10.1111/j.1365-2486.2008.01625.x.

Xu, X., H. Tian, and D. Hui, 2008: Convergence in the relationship of CO_2 and N_2O exchanges between soil and atmosphere within terrestrial ecosystems. *Global Change Biol.*, **14**, 1651–1660.

Yang, Q., H. Tian, M. A. Friedrichs, C. S. Hopkinson, C. Lu, and R. G. Najjar, 2015: Increased nitrogen export from eastern North America to the Atlantic Ocean due to climatic and anthropogenic changes during 1901–2008. *J. Geophys. Res. Biogeosci.*, **120**, 1046–1068, https://doi.org/10.1002/2014JG002763.

Zaehle, S., and A. Friend, 2010: Carbon and nitrogen cycle dynamics in the O-CN land surface model: 1. Model description, site-scale evaluation, and sensitivity to parameter estimates. *Global Biogeochem. Cycles*, **24**, GB1005, https://doi.org/10.1029/2009GB003521.

——, P. Ciais, A. D. Friend, and V. Prieur, 2011: Carbon benefits of anthropogenic reactive nitrogen offset by nitrous oxide emissions. *Nat. Geosci.*, **4**, 601–605, https://doi.org/10.1038/ngeo1207.

Zhang, B., H. Tian, C. Lu, S. R. S. Dangal, J. Yang, and S. Pan, 2017: Global manure nitrogen production and application in cropland and rangeland during 1860–2014: A 5 arcmin gridded global dataset for Earth system modeling. *Earth Syst. Sci. Data*, **9**, 667–678, https://doi.org/10.5194/essd-2017-11.

Zhang, K., C. H. Peng, M. Wang, X. L. Zhou, M. X. Li, K. F. Wang, J. H. Ding, and Q. A. Zhu, 2017: Process-based TRIPLEX-GHG model for simulating N_2O emissions from global forests and grasslands: Model development and evaluation. *J. Adv. Model. Earth Syst.*, **9**, 2079–2102, https://doi.org/10.1002/2017MS000934.

Zhang, Y., C. Li, X. Zhou, and B. Moore, 2002: A simulation model linking crop growth and soil biogeochemistry for sustainable agriculture. *Ecol. Modell.*, **151**, 75–108, https://doi.org/10.1016/S0304-3800(01)00527-0.

Zhu, Q., and Coauthors, 2014: Modelling methane emissions from natural wetlands by development and application of the TRIPLEX-GHG model. *Geosci. Model Dev.*, **7**, 981–999, https://doi.org/10.5194/gmd-7-981-2014.

Zhuang, Q., Y. Lu, and M. Chen, 2012: An inventory of global N_2O emissions from the soils of natural terrestrial ecosystems. *Atmos. Environ.*, **47**, 66–75, https://doi.org/10.1016/j.atmosenv.2011.11.036.